Rapid computation of acoustic fields in three-dimensional ocean environments

W. A. Kuperman, Michael B. Porter,[a] and John S. Perkins
Naval Research Laboratory, Washington, DC 20375

Richard B. Evans
Science Applications International Corporation, New London, Connecticut 06320

(Received 8 March 1990; accepted for publication 2 August 1990)

Adiabatic and coupled-mode theory is amenable to precalculations that can subsequently be used in a nonredundant manner to perform rapid three-dimensional acoustic field computations for a complex ocean environment. Algorithms have been developed to take advantage of both horizontal and vertical precalculated quantities. Complex three-dimensional field computations are then reduced to "spreadsheet" type manipulations of partial solutions to the wave equation. The method is illustrated by applying it to a Gulf Stream environment near the continental shelf. Results from adiabatic, coupled-mode, and parabolic-equation computations are compared.

PACS numbers: 43.30.Bp, 43.20.Ks, 92.10.Vz

INTRODUCTION

Two-dimensional, range-dependent, wave-theory propagation modeling techniques were introduced into underwater acoustics with the split-step parabolic-equation (PE) method.[1] The boundary value wave equation is approximated by the initial value PE and then rapidly solved by a multiple application of fast Fourier transforms (FFTs). Subsequent methods have altered the solution algorithm but the *marching* nature of the solution technique is intrinsic to PE approaches. A straightforward extension to three-dimensional (3-D) ocean acoustic modeling over large ocean areas takes us immediately to and beyond the limit of the present generation of computers.

The computational issues and difficulties central to the 3-D ocean acoustic modeling problem have already been highlighted in previous papers.[2-6] Many of these issues arise from the marching nature of the algorithms employed; different source/receiver configurations relative to the environment require recomputation of the total acoustic wave equation solution. Three-dimensional variation of the environment is associated with two features: the ocean bottom and oceanography. About these we make the following observations: topographical features are stationary and even the ocean medium as represented by the sound-speed profile is typically static below certain depths, depending on the particular oceanographic conditions. Traditional marching algorithms are in a sense redundant in that they fail to take advantage of the stable parts of the problem. This redundancy is particularly unattractive when the environment remains constant and only the source/receiver positions change.

Adiabatic and coupled-mode theory is amenable to precalculations that can subsequently be used in a nonredundant manner to perform rapid three-dimensional acoustic field computations in a complex ocean environment. Algorithms have been developed to take advantage of both horizontal and vertical precalculated quantities. Horizontally, we grid the ocean environment in terms of its local acoustic eigenvalues and normal modes. Though many grid points may be required to represent an environment, the number of *distinct* local environments is much smaller. For example, if we select some grid points along a bottom contour, then as long as the water column and sediment do not vary, all of these points will be identical "acoustically." We further take advantage of the deep stability of the ocean in the mode calculation by precalculating an impedance function that is a composite of the local bottom type, bottom depth, and sound-speed profile below the impedance surface. The local modes are finally obtained by "shooting" down from the ocean surface to the impedance surface. The combination of these two techniques allows complicated 3-D features requiring a large set of grid points to be built up from a smaller set of impedance functions. Furthermore, realigning the upper ocean structure with the appropriate grid structure allows for rapidly computing acoustic fields for a dynamic ocean. The acoustic field is then calculated by either an adiabatic or a coupled-mode method; in the latter case, the coupling matrices can also be precomputed and stored.

All of the above precomputed quantities are independent of source/receiver configuration. The main computation we wish to emphasize is the fast adiabatic calculation for new source/receiver positions, which comes from having precomputed the local normal modes. This allows the acoustic field for a changed source/receiver configuration to be recalculated with minimum effort as opposed to the total recalculation necessary in any marching algorithm. Speedup over conventional marching algorithms is then accomplished by using this "spreadsheet"-type approach of manipulating wave equation precalculations for adiabatic and coupled-mode methods. Horizontal refraction will be addressed in a subsequent paper, although it is included to some extent in the $N \times 2D$ approach discussed in this paper via the phase accumulation along different radials. It is im-

[a] Present address: SACLANT Undersea Research Centre, La Spezia, Italy.

 0001-4966/91/010125-09$00.80

portant to note that with this type of approach, it is not necessary to compute the acoustic field at all points along a radial if the solution is only wanted at the end point. For example, if one wants to generate a replica field on a receiver array for matched-field processing, it is possible to compute the field on the elements of the array only. The speedup is particularly evident when the additional mode-coupling or horizontal refraction computations need not be performed. In practice, this is true in the majority of cases.

In the next section, we discuss the formulations on which our computations are based. In the following section, we present several solutions to a large-scale, complex propagation problem and discuss some of the implications of the results. The region for this study is a wide geographic area containing a Gulf Stream environment off the North American continental shelf. Finally, in Sec. III, we point out relevant remaining issues that should prove to be fruitful areas for further investigation.

I. FORMULATION

In this section, we discuss adiabatic and forward coupled normal mode theory on which our calculations are based. See the Appendix for further discussion on normal mode calculations using precomputed impedance functions.

A. Adiabatic normal modes

Our starting point is the Helmholtz equation in three dimensions,

$$\rho\nabla\cdot(\nabla p/\rho) + \{\omega^2/[c^2(x,y,z)]\}p = -\delta(x,y,z), \quad (1)$$

where ω is the circular frequency of the source, $c(x,y,z)$ is the ocean sound speed, ρ is the density, and $p(x,y,z)$ is the acoustic pressure.

The normal mode solution, when $c(x,y,z) = c(z)$, is

$$p(r,z) = \frac{i}{4}\sum_{n=1}^{N} u_n(z_s)u_n(z)H_0^{(1)}(k_n r), \quad (2)$$

or, using the asymptotic approximation to the Hankel function,

$$p(r,z) = \frac{i}{4}\sqrt{\frac{2}{\pi}}e^{-i\pi/4}\sum_{n=1}^{N} u_n(z_s)u_n(z)\frac{e^{ik_n r}}{\sqrt{k_n r}}, \quad (3)$$

where r denotes the range from the source and $u_n(z)$ satisfies

$$\rho(z)\frac{d}{dz}\left(\frac{1}{\rho(z)}\frac{d}{dz}u_n(z)\right) + \left(\frac{\omega^2}{c^2(z)} - k_n^2\right)u_n(z) = 0,$$

$$u_n(0) - \frac{1}{\rho(0)}Z^T(k_n^2)\frac{du_n}{dz}(0) = 0,$$

$$u_n(h) - \frac{1}{\rho(h)}Z^B(k_n^2)\frac{du_n}{dz}(h) = 0,$$

$$\int_0^h \frac{[u_n(z)]^2}{\rho(z)}dz + \frac{1}{2k_n}\frac{d}{dk}\left(\frac{1}{Z^T}\right)u_n^2(0) - \frac{1}{2k_n}\frac{d}{dk}\left(\frac{1}{Z^B}\right)u_n^2(h) = 1. \quad (4)$$

The middle two equations represent general impedance boundary conditions with $Z^T(k^2)$ defining the surface condition, $Z^B(k^2)$ defining the bottom condition, and the squared eigenvalues k_n^2 appearing as arguments. In the following we assume, for simplicity, that the ocean surface is a free surface, $Z^T = 0$. The bottom impedance boundary condition will be used to represent an interface at depth h where the pressure and the vertical component of the particle velocity are continuous. It is assumed that the ocean is static below the depth h. The impedance function formulation is used (rather than the equivalent continuity conditions) because the impedance function can be precomputed as discussed in the Appendix. The derivation of the normalization condition may be found in Ref. 7.

The generalization of this result to *range-dependent* problems is straightforward. The adiabatic mode theory result is[8]

$$p(r,z) = \frac{i}{4}\sqrt{\frac{2}{\pi}}e^{-i\pi/4}\sum_{m=1}^{M(r)} u_m(z_s;0)u_m(z;r) \times e^{i\int_0^r k_m(s)ds}/\sqrt{k_m(r)r}. \quad (5)$$

The modal sum is over the minimum number $M(r)$ of propagating modes that exist between source and the receiver. The sum involves the *local modes* at the source $u_m(z_s;0)$ at range $r = 0$, and at the receiver $u_m(z;r)$ at range r. In practice, the calculation of modes can be somewhat computationally intensive. In order to minimize the recalculation of modes, the environment is subdivided at points $r = r_j$, $j = 1,\ldots,J_\rho$, where J_ρ denotes the number of points where the environment changes. (In a physical problem, such breaks might be placed at each range where a new sound-speed measurement has been made.) Then one solves for a set of modes at each r_j and uses linear interpolation to construct modes at ranges that lie between those r_j where the modes have been calculated.

The $N\times 2D$ generalization for a three-dimensionally varying environment is to solve the 3-D problem on N azimuthal slices as if each slice of the sound-speed profile and bathymetry profile were derived from a cylindrically symmetric problem. This approach has also been applied in parabolic-equation modeling.[4] The normal mode result is

$$p(r,z,\theta) = \frac{i}{4}\sqrt{\frac{2}{\pi}}e^{-i\pi/4}\sum_{m=1}^{M(r,\theta)} u_m(z_s;0,0)u_m(z;r,\theta) \times e^{i\int_0^r k_m(s,\theta)ds}/\sqrt{k_m(r,\theta)r}, \quad (6)$$

where the quantities in Eq. (6) also satisfy Eq. (4) parametrized with the azimuthal variable θ.

To compute the modes at discrete points, we have followed two different gridding schemes—one based on triangular elements, the other on rectangular elements. With the triangular scheme, the values of $u_m(z,r,\theta)$ and $k_m(r,\theta)$ are constructed by bivariate linear interpolation. The nodes of the triangles may be arbitrarily located. However, we have found it convenient to distribute them along isobaths. This enables extremely complicated bottom profiles to be treated with a minimum number of sets of modes—there may be many nodes on a given isobath, which will all be represented acoustically by the same set of modes (assuming no sound-speed change). With the rectangular grid we can choose to hold the environment (and hence the local modes) constant throughout each rectangle or we can interpolate along the

propagation path by first interpolating along the sides which the path crosses. Although the rectangular scheme may require more, smaller elements, many elements will still be acoustically identical. The rectangular scheme is convenient for the mode-coupling computations discussed in the next section and is also useful in computing the fields from surface generated noise.[9] We rely on the KRAKEN[10-12] normal mode program to produce the local modes for each environment.

B. Outgoing coupled modes

The spatial interpolation of mode functions and horizontal wave numbers, used with the adiabatic approximation, is done on a *mode-for-mode* basis. This interpolation excludes coupling between different modes. Mode coupling requires a scheme that does not spatially interpolate on a *mode-for-mode* basis. The rectangular scheme, which holds the environment constant in each rectangle, lends itself to a straightforward generalization to outgoing stepwise coupled modes[13] for the $N \times 2D$ case. The one-way theory assumes that the solution is outgoing and matches only the pressure at interfaces between environmental regions. The mode amplitudes are initialized at the source and advanced in range using the horizontal wave numbers for each mode. When a new environmental region is encountered, the mode-coupling matrix is applied to the vector of mode amplitudes. Then, the mode amplitudes are advanced with the new horizontal wave numbers. The adiabatic approximation replaces the coupling matrix with a diagonal matrix, which contains ratios of square roots of the horizontal wave numbers in adjacent regions.

Consider the two-region problem shown in Fig. 1, where the environment changes at $r = r_1$. The discrete dependence of the environment on range will be indicated by a subscript designating region one or region two. In the case of the mode functions and the horizontal wave numbers, a different symbol will be used for region one and region two. This is in contrast to the continuous dependence indicated by the notation in the adiabatic case.

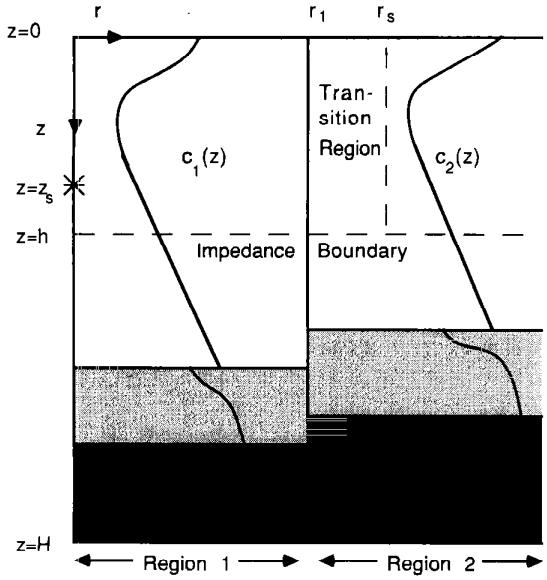

FIG. 1. A two-region propagation problem with a transition region for smoothing an abrupt environmental change.

The normal mode solution in region one, containing the source, is

$$p_1(r,z) = \sum_{n=1}^{N} s_n \psi_n(z) \frac{e^{i\alpha_n r}}{\sqrt{r}}, \tag{7}$$

where ψ_n are the modes and α_n are the corresponding wave numbers in region one. The mode excitation s_n is determined by the source depth through the equation

$$s_n = (i/4)\sqrt{2/\pi\alpha_n}\, e^{-i\pi/4} \psi_n(z_s). \tag{8}$$

The outgoing stepwise coupled normal mode solution in region two is

$$p_2(r,z) = \sum_{m=1}^{M} b_m \phi_m(z) \frac{e^{i\beta_m(r-r_1)}}{\sqrt{r}}, \tag{9}$$

where ϕ_m are the modes and β_m are the corresponding wave numbers in region two. The coefficients b_m will be determined by mode matching at r_1. It is convenient to express the field in region one at r_1 by

$$p_1(r_1,z) = \sum_{n=1}^{N} \frac{a_n \psi_n(z)}{\sqrt{r_1}}, \tag{10}$$

where

$$a_n = s_n e^{i\alpha_n r_1}. \tag{11}$$

The coefficients a_n include the effect of the phase change between 0 and r_1. The mode matching condition at $r = r_1$, using Eqs. (9) and (10), then becomes

$$\sum_{n=1}^{N} a_n \psi_n(z) = \sum_{m=1}^{M} b_m \phi_m(z). \tag{12}$$

The coefficients a_n are known; the coefficients b_m are found as follows. Equation (12) is multiplied by $\phi_m/\rho_2(z)$ and integrated over the interval $[0,h]$ to give

$$\sum_{m'=1}^{M} d_{m,m'} b_{m'} = \sum_{n=1}^{N} f_{m,n} a_n, \tag{13}$$

where

$$d_{m,m'} = \int_0^h \frac{\phi_m(z)\phi_{m'}(z)}{\rho_2(z)}\, dz \tag{14}$$

and

$$f_{m,n} = \int_0^h \frac{\phi_m(z)\psi_n(z)}{\rho_2(z)}\, dz. \tag{15}$$

In matrix–vector notation, Eq. (13) has the form

$$D\mathbf{b} = F\mathbf{a}, \tag{16}$$

where $\mathbf{a} = [a_1,...,a_N]^T$, $\mathbf{b} = [b_1,...,b_M]^T$, D is an $M \times M$ matrix containing the $d_{m,m'}$ values, and F is an $M \times N$ matrix containing the $f_{m,n}$ values. The integration in Eq. (14), needed to compute D, can be avoided when $m \neq m'$ by using

$$d_{m,m'} = \frac{\phi_m(h)d\phi_{m'}(h)/dz - \phi_{m'}(h)d\phi_m(h)/dz}{\rho_2(h)(\beta_{m'}^2 - \beta_m^2)}, \quad m \neq m'. \tag{17}$$

Equation (17) follows from Lagrange's identity

$$\frac{d}{dz}\left[\phi_m\left(\frac{1}{\rho_2}\frac{d\phi_{m'}}{dz}\right)-\phi_{m'}\left(\frac{1}{\rho_2}\frac{d\phi_m}{dz}\right)\right]$$

$$=(\beta^2_{m'}-\beta^2_m)\frac{\phi_m\phi_{m'}}{\rho_2} \tag{18}$$

that can be derived from the differential equation for the mode functions. The diagonal elements in D can be obtained from the normalization condition in Eq. (4).

Equation (16) is solved for **b** to obtain

$$\mathbf{b}=D^{-1}F\mathbf{a}. \tag{19}$$

The matrix $C=D^{-1}F$ is the coupling matrix that projects ψ_n onto ϕ_m. If the ϕ_m are orthogonal on the interval $[0,h]$, then D is the identity matrix and the elements in C are obtained from the integral in Eq. (15). If the ϕ_m are nearly orthogonal, then D is near the identity matrix and the matrix D^{-1} can be approximated easily by

$$D^{-1}=(I-E)^{-1}\cong I+E. \tag{20}$$

The coupled-mode calculation requires the interval $[0,h]$ be a significant part of the water column. It does not benefit from the precalculation of the impedance function to the extent that the adiabatic calculation does.

An abrupt change in the environment at r_1 can introduce a sudden change in the field. This is eliminated by smoothing the field in a transition region shown in Fig. 1. The field in the region $r_1 \leqslant r \leqslant r_s$ is computed using

$$p(r,z)=\frac{(r_s-r)}{(r_s-r_1)}p_1(r,z)+\frac{(r-r_1)}{(r_s-r_1)}p_2(r,z). \tag{21}$$

In this way, the field from region one is partly retained in the transition region and the field in region two does not take full effect until $r \geqslant r_s$.

The above analysis can easily be applied to multiple regions. Suppose a new region is encountered at $r_2 > r_1$. The vector **b** replaces the source excitation vector **s**. The phase of **b** is advanced over the interval from r_1 to r_2 defining a new vector **a** at r_2. Then the process is repeated using Eq. (19) to generate another vector **b** for the new region.

II. A GULF STREAM EXAMPLE

In order to demonstrate some of the ideas discussed above, we consider a large-scale, realistic problem with both bathymetric and oceanographic variations. In Fig. 2 we have taken bathymetric contours, made from the SYNBAPS database,[14] for a 650-km square off the east coast, and have shaded (in blue) the approximate position of the Gulf Stream, as it was in March 1983.[15] The positions of two cold-core eddies, and a small seamount, are also shaded. We chose five historical profiles to represent the sound-speed variations across the Gulf Stream. In Fig. 3 we show the environment along a track from the center of the region to the northwest. These same profiles were used to represent the eddies. To perform the several computations we have been discussing, it is necessary to represent this environment in different ways. We will describe how this was done for each type of calculation.

An $N\times 2D$ adiabatic solution is displayed in Fig. 4. A 50-Hz source is located at position $x=333$ km, $y=315$ km,

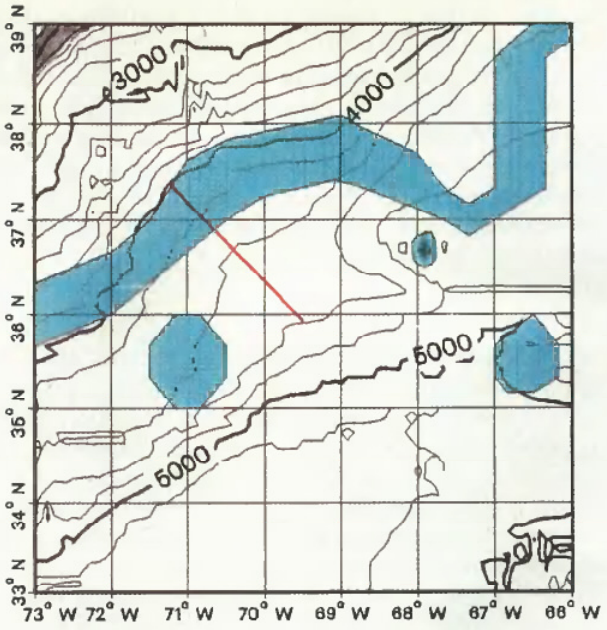

FIG. 2. Gulf Stream environment used for the examples. The Gulf Stream, two cold-core eddies, and a small seamount are shaded in blue over the bathymetric contours. The red line indicates the track of the vertical sound-speed structure shown in Fig. 3.

and depth $z=100$ m. In order to make comparisons with an $N\times 2D$ parabolic-equation (PE) result, we chose to display all solutions by computing the acoustic field at evenly spaced points along radials at a fixed depth of 217 m. The pressure values at a depth of 217 m (a depth where there was a computational grid point for the PE) were saved along 65 radials every 0.25 km (the PE *computational* range step was 25 m). The computational radials spanned 360 deg, and were spaced 5.625 deg apart. The magnitude-squared pressure values were smoothed with a 5-km Gaussian-weighted window along each radial, converted to transmission loss (TL), and then interpolated onto a rectangular 1- $\times$1-km grid over the entire 650- $\times$650-km region. These values were then plotted using a 12-level color scale representing 80 to 98 dB

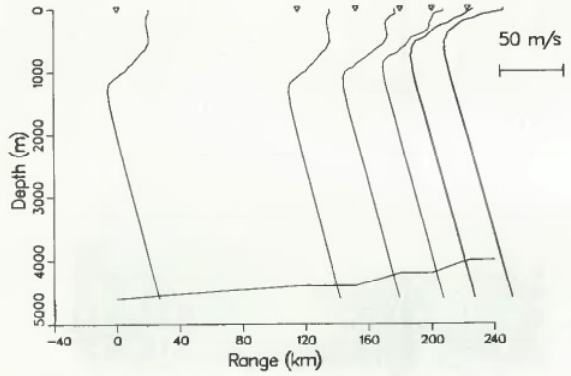

FIG. 3. Sound-speed profiles and bathymetry along the track shown in red on Fig. 2. The dels indicate the ranges of the profiles from the endpoint near the center of the region and each nabla is positioned over the 1500-m/s point of the profile.

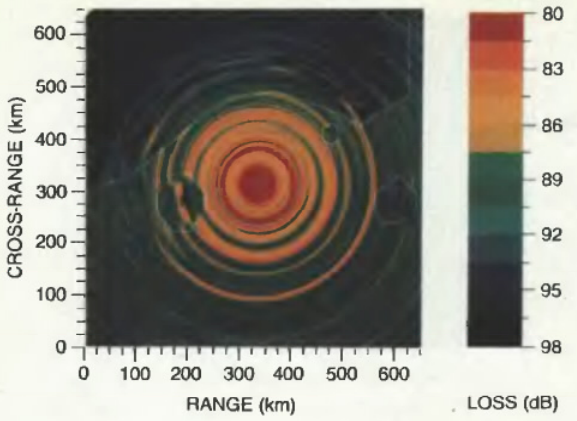

FIG. 4. The $N \times 2D$ adiabatic mode result at a depth of 217 m computed with the triangular grid shown in Fig. 5.

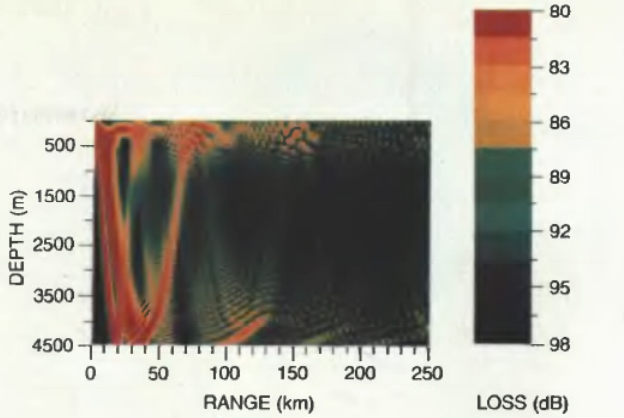

FIG. 6. Transmission loss in the vertical plane extending from the source to the northwest.

with red 80 dB or less, and black 98 dB or more; each color level spans 1.5 dB. The resulting 3-D acoustic fields provide a type of "acoustic image" of the environment.

In Fig. 4, the outlines of the Gulf Stream, the two eddies, and the small seamount are overlaid on the plot of the data. This is our initial calculation and is made using a triangular grid of approximately 450 points and 830 triangles as shown in Fig. 5. The grid was constructed along the contours seen in Fig. 2. The important point, however, is that, even though this is a rather complex 3-D environment, there were only 54 distinct local environments, and therefore only 54 sets of modes to compute and store for subsequent calculations. If the shallow areas (below, say, 3000 m) are not included, only about ten impedance functions are needed, and when they are matched with the five profiles, about 40 distinct mode files result.

Since the region to the southeast is reasonably flat and has no oceanographic features, this part of Fig. 4 has a cylindrical symmetry as one would expect. The eddies break this symmetry, and the effect of the Gulf Stream is to produce generally greater loss on the far side. This does not mean that the Gulf Stream is acting like an acoustic "wall"; the energy is being redistributed to other depths or being absorbed by the bottom.

Figure 6 is a color contour of the transmission loss in the vertical plane extending from the source to the northwest.

In order to compute an $N \times 2D$ mode-coupling result, we need an environment that is constant over small rectangular patches. The mode coupling will then occur at the transition from one patch to the next. The entire region was divided into 10- $\times$ 10-km squares. Each square was assigned a set of local modes by finding the node on the triangular grid that was closest to the center of the square—the set of modes

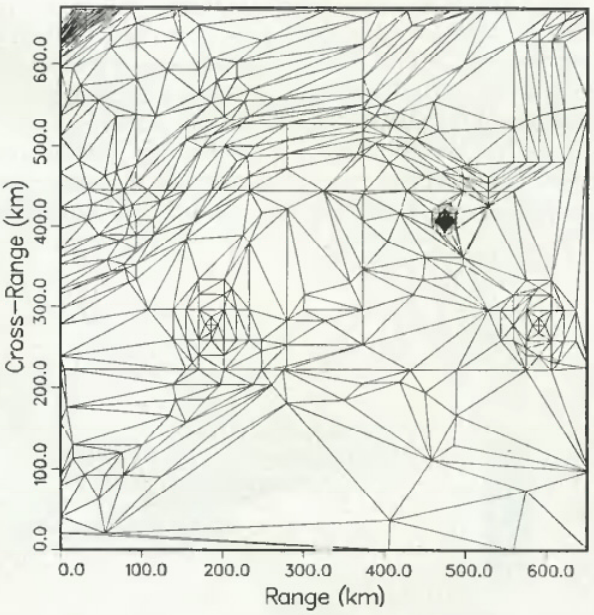

FIG. 5. Triangular discretization of the Gulf Stream environment shown in Fig. 2.

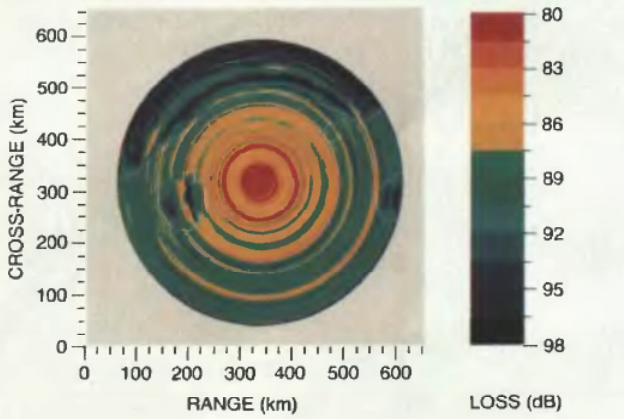

FIG. 7. The $N \times 2D$ adiabatic mode result at a depth of 217 m computed with a rectangular discretization of the Gulf Stream environment shown in Fig. 2. Compare to the triangular result in Fig. 4 and the coupled-mode result in Fig 8.

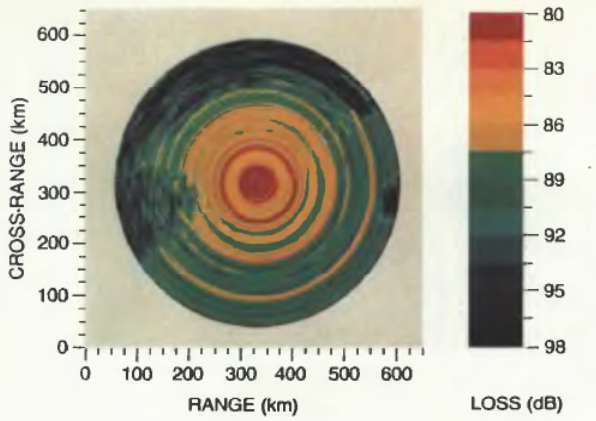

FIG. 8. The $N \times 2D$ coupled-mode result at a depth of 217 m computed with rectangular discretization of the Gulf Stream environment shown in Fig. 2. Compare to the adiabatic result in Fig. 7.

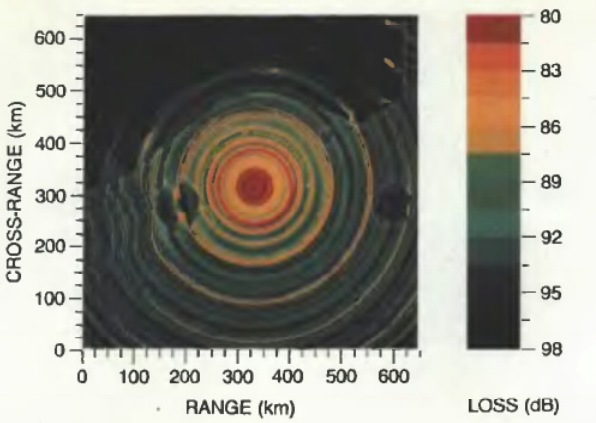

FIG. 10. An adiabatic mode result computed by dividing the region into 0.5-km squares and computing the TL to the center of each square.

corresponding to that node was assigned to that square.

Because the environment for which the solution is being computed is not exactly the same as it was for Fig. 4, we recomputed the adiabatic result. This result is shown in Fig. 7. That is, Figs. 4 and 7 are both $N \times 2D$ adiabatic calculations, but they used different views of the discrete environmental data of Fig. 2.

To do the mode-coupling calculation, it was necessary to consider all combinations of pairs of adjacent environments and compute and store the coupling matrices of Eq. (15) (the mode functions were essentially orthogonal over the depth interval used in the calculation). Since the shallow region to the northwest was relatively uninteresting, we decided to reduce the range of the computation, thereby avoiding the necessity of computing and storing the coupling matrices relevant only to that region. In total, we ended up with 96 pairs of environments. This requires 192 coupling matrices. However, in this problem we did not use any density changes so that the coupling matrix for moving from environment "A" to environment "B" is the transpose of the matrix for moving from environment "B" to environment "A" [see Eq. (15)]. Each matrix required about 30 min of computation time on a VAX 11/785. The final mode-coupling solution in Fig. 8 required about 90 min of computation time, surprisingly close to the 50 min for the (longer-range) adiabatic computation in Fig. 4.

The structure of the coupling matrices is interesting. In Fig. 9(a) we have color coded the entries for the matrix, which couples the modes from a depth of 3200 m to a depth of 3400 m using a constant sound-speed profile (the cold-water profile at the end of the track in Fig. 3). Figure 9(b) displays the matrix that couples two of the Gulf Stream profiles (the third and fourth profiles on the track in Fig. 4) at a depth of 4200 m. Both matrices of Fig. 9 are banded, indicating that the computation could be made more efficient by using only a band centered on the diagonal. Also, this reduces the computing and storage requirements of the matrices themselves.

Figure 9(a) and (b) is different in that, as you move away from the main diagonal, the values monotonically decrease in Fig. 9(a) while, in Fig. 9(b), the structure is more complex. Bathymetry changes affect the higher-order modes only, whereas the oceanographic effects are distributed over all modes. As noted above, the adiabatic approximation effectively replaces the coupling matrices with diagonal matrices. Figure 9(a) shows a matrix that is almost diagonal, especially in the lower-order modes. Figure 9(b), on the other hand, indicates that the coupling between these two profiles may be too complex for the adiabatic approximation.

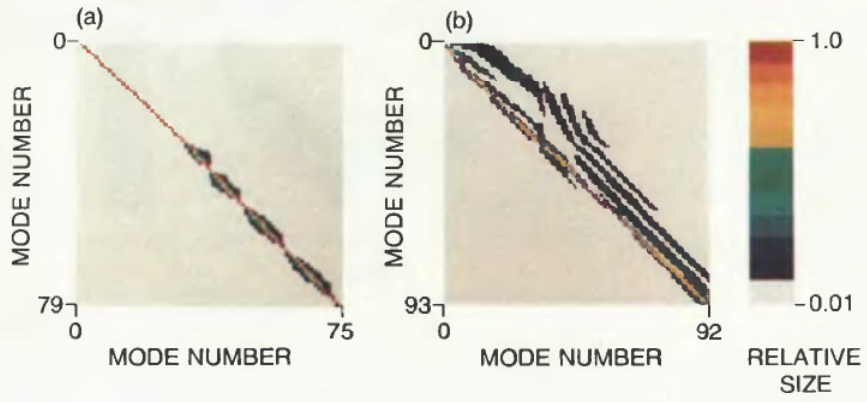

FIG. 9. Mode-coupling matrix for (a) a change in depth from 3200 to 3400 m using the cold-water profile at the end of the track in Fig. 3, and (b) two Gulf Stream profiles (the third and fourth profiles on the track in Fig. 3) at a depth of 4200 m.

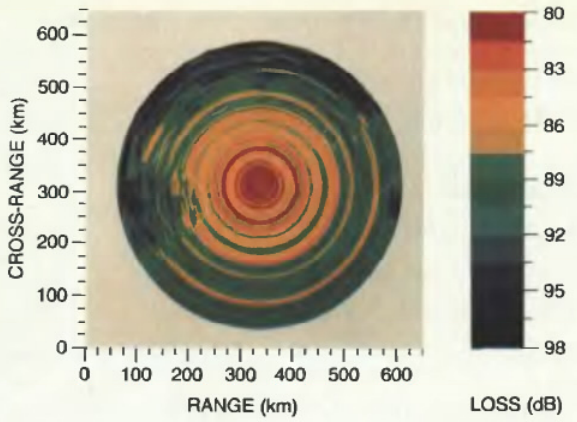

FIG. 11. The $N \times 2D$ split-step parabolic-equation solution at a depth of 217 m computed by inputting the bathymetry and sound speeds at the nodes of Fig. 5.

Thus it is possible to precompute these matrices, and when the coupling is complex—include the coupling; otherwise, use the adiabatic approximation.

We wish to show an additional adiabatic computation. We divided the entire region into 0.5×0.5-km squares in the same manner described above. Instead of computing along radials, we computed the TL to the center of each square. This result is shown in Fig. 10 and is significant in that, at least to a resolution of 0.5 km, no features of the environment are "missed" in the calculation. Again, with the adiabatic normal mode approach, the field can be computed directly at the desired receiver points without marching the solution through the environment.

In Fig. 11 we present an $N \times 2D$ split-step PE calculation[16] for this problem. It happens that this implementation inputs the environmental description on a triangular grid. We used the same triangular grid of Fig. 5; however, now it is sound-speed data that is input for each node, and there is an internal interpolation scheme to produce index of refraction values on the *computational* grid, which is cylindrical. Thus, although these two computer models use essentially the same input data, it is difficult to attribute differences in the solutions they produce to differences in theory or differences in numerical implementation. Figure 12 shows the difference between (a) the PE computation and the adiabatic result and (b) the PE computation and the coupled-mode result, and we note that the coupled-mode and PE solutions are very similar. The larger differences seen in the circular arcs to the southeast of the source result from a range shift in the convergence zones, rather than differences in intensity levels. At any rate, the difference between reality and any of these large-area solutions is probably dominated by our inability to obtain detailed synoptic 3-D information about the ocean and sediments. We also computed the full 3-D PE solution[4,16] and obtained essentially identical (within 0.15 dB) results as those shown in Fig. 11. However, the angular spacing used (5.625 deg) could have been too large to obtain improved results.

III. SUMMARY AND CONCLUSIONS

We have described approaches to the problem of computing acoustic fields in three-dimensional ocean environments that involve computing and storing local modal information throughout a (large) region. Propagation from any source position to any receiver position can then be computed very rapidly.

Our standard or baseline solution makes use of a triangular patchwork with modes defined at the corners of the triangles, and invokes the $N \times 2D$ approach in which the ray paths are straight lines when viewed in plan. The mode structure itself is computed rapidly with the use of precalculated impedance functions (see the Appendix) that are obtained by taking advantage of the stability of the lower part of the deep ocean. Furthermore, adiabatic mode theory is used to compute the acoustic field along a radial.

Extremely complicated 3-D problems can be treated in this fashion with relatively modest computer effort. For instance, in the Gulf Stream example we showed an oceanographically active environment of approximately 650 km on a side. The 450 nodes used to define the environment required only 54 distinct environmental data sets and sets of local modes. We have also shown that outgoing stepwise coupled-mode solutions can be generated much more rapidly than was previously believed with a rectangular grid of precalculated modes and mode-coupling matrices.

The capability to compute 3-D acoustic fields in complex environments and thereby produce "acoustic images" poses additional challenges concerning *realistic* accuracy

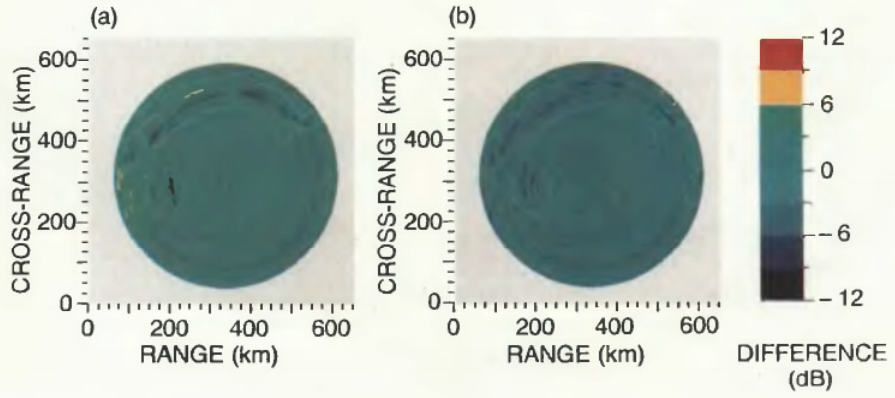

FIG. 12. Differences between (a) the PE result and the adiabatic result and (b) the PE result and the coupled-mode result.

criteria. If we use the conventional criteria (taken from computing standard 2-D transmission loss curves) in a 3-D computation, we are confronted with acquiring an inordinate amount of environmental input data. Furthermore, comparing conventional transmission loss curves is an exercise in comparing numbers, whereas images depict physical phenomenon. Missing a shift of a convergence zone by 1 km in a transmission loss curve may result in a 15-dB error that does not appear as serious in a 3-D construction of the acoustic field that displays the phenomenon over a large area. The 3-D picture of the acoustic field taken with the uncertainty normally associated with real environmental data seems to require some relaxation of the accuracy one normally seeks in computing transmission loss curves. Certainly, it calls into question the value of the additional information one may gain for substantial increases in computation costs (as when using mode coupling).

A remaining issue is that of the need for mode coupling, i.e., the shortcomings of the adiabatic approximation. It is not clear whether horizontal refraction or mode coupling is more important. One can, however, construct cases where horizontal refraction is nonexistent and mode coupling important—for instance, a seamount in a 2-D model can cause significant mode coupling and the corresponding azimuthally symmetric problem has no horizontal refraction. A subsequent paper will deal with horizontal refraction but we note here that the $N \times 2D$ computation contains horizontal refraction via the different phase accumulation along individual radials. This can be thought of as being the lowest-order inclusion of cross-range variability in the same sense that the PE equation includes range dependence although originally derived by considering only a stratified medium.

APPENDIX: PRECALCULATION OF IMPEDANCE SURFACES

In this Appendix we show how to reduce the redundancy inherent in the mode computations. Thus the static part of the problem, which includes both the ocean bottom and a significant portion of the water column, is replaced by an impedance function. In a typical deep water problem, approximately 90% of the water column can be removed by precalculation. This impedance surface then forms the lower boundary condition for a much reduced modal computation.

Suppose that the ultimate bottom boundary condition for the differential equation in Eq. (4) is a rigid bottom at some great depth $z = H$ as shown in Fig. 1 or a radiation condition with $H \to \infty$. The wave numbers (eigenvalues) can be found by shooting down from the surface and up from H and choosing the wave number to satisfy the continuity conditions at $z = h$.

Let u and v be solutions of the differential equation in Eq. (4) that satisfy the surface boundary condition at $z = 0$ and the bottom boundary condition at $z = H$, respectively. The continuity conditions at $z = h$ are

$$u(h) = v(h), \tag{A1}$$

$$u'(h)/\rho(h^-) = v'(h)/\rho(h^+). \tag{A2}$$

The solution v can always be normalized to satisfy one of the continuity conditions independent of the wave number. If the wave number is chosen such that (provided zeros and infinities are interpreted correctly)

$$u(h)/[u'(h)\rho(h^+)] = v(h)/[v'(h)\rho(h^-)], \tag{A3}$$

then the other continuity condition will also be satisfied. This is equivalent to

$$u(h) - [1/\rho(h^-)]Z^B(k^2)u'(h) = 0, \tag{A4}$$

where the impedance function is given by

$$Z^B(k^2) = v(h)\rho(h^+)/v'(h). \tag{A5}$$

It is not even necessary to know the appropriate normalization for v.

The impedance function in Eq. (A5) depends only on the static part of the environment below $z = h$. From a practical point of view the impedance function is computed at a set of points, $k_l = k_{\min} + l\delta k$. The number of k points and the interval they cover are determined using the same considerations as for a spectral integral code.[17] In subsequent calculations, the impedance at an arbitrary k value is obtained by polynomial interpolation.

Here, we illustrate the impedance function method for the two profiles in Fig. A1. The second profile can be thought of as coming from a change in the upper part of the ocean, for instance, an eddy moving over the same location. The two profiles are identical below 1500 m. The solid line in Fig. A2(a) is the impedance function evaluated at a depth of 1500 m obtained by shooting up from the bottom through the lower 3500 m of the water column using the profile in Fig. A1(a). The dashed line is the impedance function at the same 1500-m depth obtained by shooting down from the ocean surface. The intersection of the two functions occurs at the eigenvalues of the total problem. The locations of the eigenvalues obtained from a straightforward eigenvalue

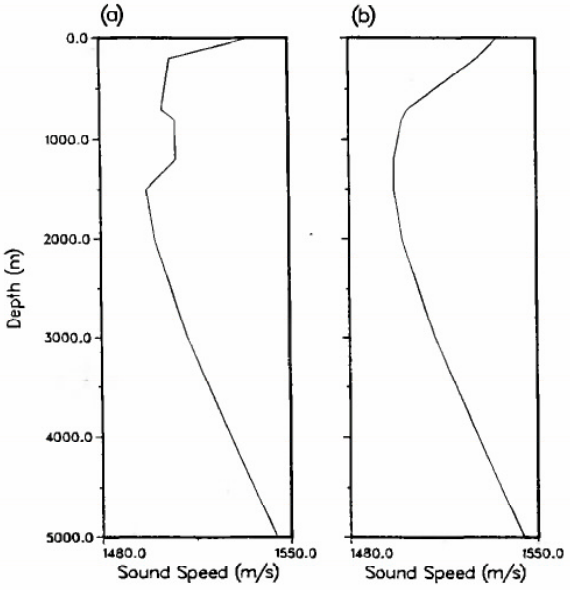

FIG. A1. Two profiles used to demonstrate the use of the impedance surface.

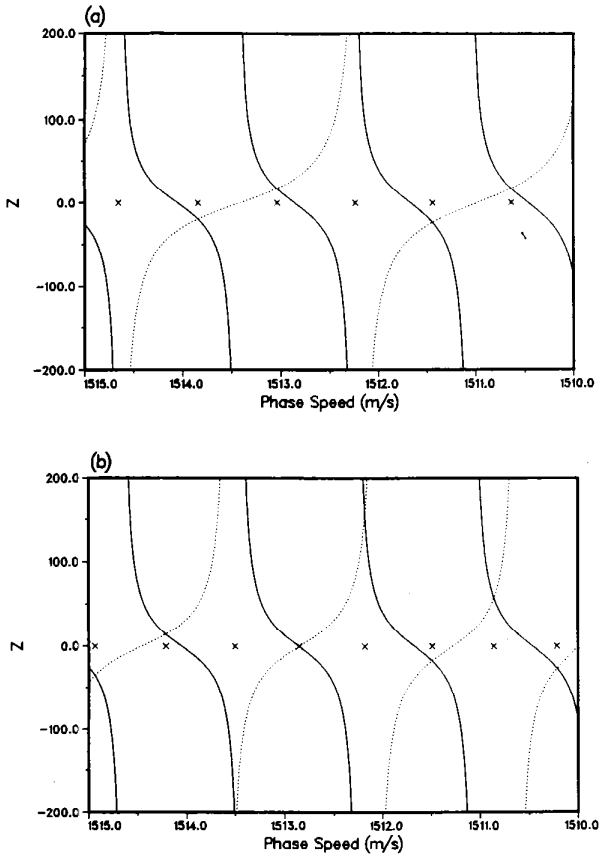

FIG. A2. Impedance functions for the profiles in Fig. A1. The solid line is the impedance function evaluated at a depth of 1500 m obtained by shooting up from the bottom. The dashed line is the impedance function at 1500 m obtained by shooting down from the surface using (a) the profile in Fig. A1(a) and (b) the profile in Fig. A1(b). The locations of the eigenvalues obtained from a straightforward eigenvalue search are indicated by the "×'s."

search is indicated by the "×'s." Now, changing to the profile indicated in Fig. A1(b) requires only the upper computation to be redone for the total eigenvalue search. This new computation is shown in Fig. A2(b), where the solid line is identical to that of Fig. A2(a). Hence, with the solid line taken as the "precalculated" stable part of the problem, we have reduced the eigenvalue search to the simpler, shallower problem. In this case there was a reduction of 70% in computational effort over the full mode problem. Typically, the reduction factor is more than 90% for deep water problems.

When elastic layers are present, we propagate the impedance coefficients using the compound matrix method as described in Ref. 11. In addition, we observe that the technique may be applied to static parts of the problem even if such layers are sandwiched between dynamic layers. In this case, one computes a pair of linearly independent solutions and from them a propagator matrix for the static layer.

The procedure is applicable to spectral integral codes, in fact with less effort, since much of the care taken in computing the impedance coefficients stems from the need to interface with efficient eigenvalue finding techniques. Spectral integral codes have no analogous requirement. Finally, we observe that in either modal or spectral integral implementations, the impedance sampling need not be a regular mesh and significant gains might be obtained by adaptively sampling the impedance function.

[1] F. D. Tappert, "The parabolic approximation method," in *Wave Propagation and Underwater Acoustics*, edited by Joseph B. Keller and John S. Papadakis (Springer-Verlag, Berlin, 1977), Lecture Notes in Physics, Vol. 70.

[2] A. D. Pierce, "Extension of the method of normal modes to sound propagation in an almost-stratified medium," J. Acoust. Soc. Am. **37**, 19–27 (1965).

[3] H. Weinberg and R. Burridge, "Horizontal ray theory for ocean acoustics," J. Acoust. Soc. Am. **55**, 63–79 (1974).

[4] J. S. Perkins and R. N. Baer, "An approximation to the three-dimensional parabolic-equation method for acoustic propagation," J. Acoust. Soc. Am. **72**, 515–522 (1982).

[5] W. L. Siegmann, G. A. Kriegsmann, and D. Lee, "A wide-angle three-dimensional parabolic wave equation," J. Acoust. Soc. Am. **78**, 659–664 (1985).

[6] M. D. Collins and S. A. Chin-Bing, "A three-dimensional parabolic equation model that includes the effects of rough boundaries," J. Acoust. Soc. Am. **87**, 1104–1109 (1990).

[7] H. P. Bucker, "Sound propagation in a channel with lossy boundaries," J. Acoust. Soc. Am. **48**, 1187–1194 (1970).

[8] L. M. Brekhovskikh and Yu. Lysanov, *Fundamentals of Ocean Acoustics* (Springer-Verlag, Berlin, 1982).

[9] J. S. Perkins, W. A. Kuperman, F. Ingenito, and J. Glattetre, "Modeling ambient noise in three-dimensional ocean environments," J. Acoust. Soc. Am. (in preparation).

[10] M. B. Porter and E. L. Reiss, "A numerical method for ocean-acoustic normal modes," J. Acoust. Soc. Am. **76**, 244–252 (1984).

[11] M. B. Porter and E. L. Reiss, "A numerical method for bottom interacting ocean acoustic normal modes," J. Acoust. Soc. Am. **77**, 1760–1767 (1985).

[12] M. B. Porter, "The KRAKEN normal mode program," SACLANT Undersea Research Center Tech. Rep. (1990).

[13] R. B. Evans, "A coupled mode solution for acoustic propagation in a waveguide with stepwise depth variations of a penetrable bottom," J. Acoust. Soc. Am. **74**, 188–195 (1983).

[14] R. J. Vanwyckhouse, "Synthetic bathymetric profiling system (SYNBAPS)," Tech. Rep. 233, Naval Oceanographic Office (1973).

[15] J. W. Clark and S. Auer, "East Coast ocean features," Oceanogr. Monthly Summary **III**(3), 19 (March 1983).

[16] J. S. Perkins, R. N. Baer, L. F. Roche, and L. Bruce Palmer, "Three-dimensional parabolic-equation-based estimation of the ocean acoustic field," NRL Rep. 8685, Naval Research Laboratory (1983).

[17] H. Schmidt and F. B. Jensen, "A full wave solution for propagation in multilayered viscoelastic media with application to Gaussian beam reflection at fluid solid interfaces," J. Acoust. Soc. Am. **77**, 813–825 (1985).